11th World Congress on Computational Mechanics (WCCM XI)
5th European Conference on Computational Mechanics (ECCM V)
6th European Conference on Computational Fluid Dynamics (ECFD VI)
E. Oñate, J. Oliver and A. Huerta (Eds)

RESEARCH ON CAVITY FLOW AROUND UNDERWATER 3D VEHICLE BASED ON POTENTIAL FLOW THEORY

JIAOLONG.ZHAO[*1], LONGQUAN.SUN[†2], YANG.ZHANG[*3] AND HAILONG.CHEN[*4]

[*1]Harbin Engineering University (HEU)
College of Shipbuilding Engineering.
Nantong Street 145#, 150001 Harbin, China
e-mail: zhaojiaolong039@sina.com

[*3]Harbin Engineering University (HEU)
College of Shipbuilding Engineering.
Nantong Street 145#, 150001 Harbin, China
e-mail: zhaojiaolong@hrbeu.edu.cn

[†2] Harbin Engineering University (HEU)
College of Shipbuilding Engineering.
Nantong Street 145#, 150001 Harbin, China
e-mail: sunlongquan@hrbeu.edu.cn

[*4] Harbin Engineering University (HEU)
College of Shipbuilding Engineering.
Nantong Street 145#, 150001 Harbin, China
e-mail: chenhailong@hrbeu.edu.cn

Key Words: *Cavity, Underwater Vehicle, Around Flow, Potential Flow Theory.*

Abstract. On the basis of the potential flow theory, the paper establishes mathematical calculations of the cavity flow around underwater three-dimensional (3D) vehicle. The problems of partial cavity and no cavity flow around underwater vehicle were researched. And its validity was demonstrated with the comparisons between the calculation results and experiments. On the basis of it, the paper analyzed the effects of different head shape and different cavitation number to the characteristics of flow around underwater vehicle. Some laws of flow were obtained: the normal force and pressure center coefficient wasn't be in singular proportion to cone angle. The cone angle and cavitation number had a strong influence on the cavity shape and the hydrodynamic loads. The results would play a guide role in the hydrodynamic force design.

1 INTRODUCTION

The existing of cavity makes underwater vehicle bear complex hydrodynamic forces [1-3], during its operation under water. Formerly, there are two kinds of way for calculating underwater vehicle's hydrodynamic coefficients [4-5], which is cavitation water tunnel or wind tunnel tests and CFD numerical simulation. Despite of long test period and high cost, cavitation water tunnel、wind tunnel tests are the most effective method. CFD numerical simulation also needs long test period. The adoption of potential flow theory in calculating flow around underwater vehicle is a very efficient method, Leng[6] calculated underwater 2D vehicle's partial cavity feature; Hanaoka[7] solved the partial cavity problem of simple shape such as a wing by using singularities(source and sink) method; Liu and Lu[8] calculated axisymmetric objects' partial cavity problem. On the basis of 3D potential flow theory[9-10], this paper proposes a new way to calculating partial cavity flow around underwater vehicle.

2 CALCULATION MODEL

The cavitation water tunnel can make no cavity flow and partial cavity around the underwater vehicle, by adjusting the tunnel working pressure. This paper deduces and establishes two mathematical calculations of the cavity flow around underwater 3D vehicles for the different working conditions in the cavitation water tunnel.

2.1 Calculation model for no cavity flow

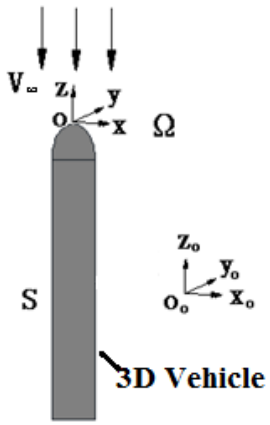

Figure 1: The model for the calculation of vehicle in no cavity flow

Figure 1 shows the mathematical model to calculate the hydrodynamic load coefficient of the vehicle in no cavity flow. We will denote the body surface by S ; the freestream velocity by U_∞ .Assuming the stream is potential flow, the freestream velocity (or infinity velocity) can be written as:

$$\vec{U}_\infty = u_{\infty x}\vec{i} + u_{\infty y}\vec{j} + u_{\infty z}\vec{k} \tag{1}$$

$\Psi(x, y, z)$ is the flow velocity potential, which is suitable for the Laplace equation in the stream, satisfies the boundary condition on the surface of the vehicle and is uniform to the freestream velocity potential at infinity:

$$\begin{aligned} &\nabla^2\Psi = 0 && \text{the whole stream} \\ &\frac{\partial\Psi}{\partial n} = u_n = 0 && \text{the vehicle's surface} \\ &\Psi \approx xu_{\infty x} + yu_{\infty y} + zu_{\infty z} && \text{infinity} \end{aligned} \tag{2}$$

The flow velocity potential can be expressed as a summation of freestream velocity potential and the disturbance velocity potential ψ:

$$\Psi \approx xu_{\infty x} + yu_{\infty y} + zu_{\infty z} + \psi \tag{3}$$

The disturbance velocity potential ψ satisfies the following conditions:

$$\begin{aligned} &\nabla^2\psi = 0 && \text{the whole stream} \\ &\frac{\partial\psi}{\partial n} = -\vec{U}_\infty \cdot \vec{n} && \text{the vehicle's surface} \\ &\psi \to 0 && \text{infinity} \end{aligned} \tag{4}$$

The boundary integral equation can be written as:

$$A\psi(\mathbf{p}_1) = \iint_S \left(\frac{\partial\psi(\mathbf{p}_2)}{\partial n} g(\mathbf{p}_1, \mathbf{p}_2) - \psi(\mathbf{p}_2) \frac{\partial}{\partial n} g(\mathbf{p}_1, \mathbf{p}_2) \right) dS \tag{5}$$

In this relation, the field point $\mathbf{p}_1$ and the source point $\mathbf{p}_2$ are both on the vehicle surface. A is the observation angle of the flow field at the point $\mathbf{p}_1$, which can be obtained in the following equation:

$$A = \iint_S \frac{\partial g}{\partial n}(\mathbf{p}_1, \mathbf{p}_2)\, dS_q \qquad \mathbf{p}_1 \in S \tag{6}$$

$g(\mathbf{p}_1, \mathbf{p}_2)$ is the 3D Green's formula $g(\mathbf{p}_1, \mathbf{p}_2) = 1/R$, in which R represents the distance between the field point $\mathbf{p}_1$ and the source point $\mathbf{p}_2$.

Once the disturbance velocity potential ψ has been obtained, the pressure on the vehicle surface can be calculated by Bernoulli equation:

$$P = \eta \left[P_\infty - \frac{1}{2}\rho(\vec{U}_\infty \cdot \nabla\psi + \nabla^2\psi) \right] \tag{7}$$

η is the vehicle surface pressure correction function, which is related to the angle of attack. The normal hydrodynamic force coefficients C_n can be obtained:

$$C_n = \frac{\int_S Pds}{1/2\,\rho \vec{U}_\infty^{\,2} S_V} \tag{8}$$

S_V is the areas of the vehicle's cross section.

2.2 Calculation model with partial cavity flow

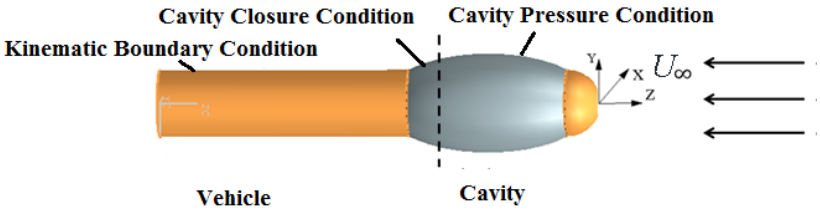

Figure 2: The model for the calculation of vehicle with partial cavity flow

Figure 2 shows the mathematical model to calculate the partial cavity flow around the vehicle. The whole flow field satisfies the Laplace equation (Eq.5). The surface of the vehicle can be divided into two regions, which is vehicle dry surface and cavity surface, according to the flow state. Near the trailing edge of the cavity, we use a cavity termination condition to make the cavity closure. Then the partial cavity satisfies the following conditions [11]:

$$\begin{cases} \dfrac{\partial \psi}{\partial n} = -\boldsymbol{U}_\infty \cdot \boldsymbol{n} \\ q_t = U_c\left[1 - f(t_f)\right] \qquad h(t_L) = 0 \\ U_c = U_\infty\sqrt{1+\sigma} \qquad \dfrac{\partial \Psi}{\partial n} = \dfrac{\partial \Psi}{\partial t}\dfrac{\partial h}{\partial t} \\ \Psi_\infty = \boldsymbol{U}_\infty \cdot \mathbf{Z} \end{cases} \tag{9}$$

L is the partial cavity length, h is the partial cavity thickness, δ is the cavitation number, t is the partial cavity length on the axis z. t_f is the partial cavity termination length, which makes the continuity of the cavity pressure condition and the kinematic boundary condition. The cavity shape and pressure can be obtained by iteratively calculate Eq.9.

3 VALIDITY OF THE MODELS' REASONABILITY

3.1 Reasonability for no cavity flow model

To verify the validity of calculation model for no cavity flow, this paper compares the predicted results with the experiment data (from Ref.4). The comparison of normal force coefficients and pressure center coefficient between predicted results and the test data as follows:

Table.1 The compare of normal force coefficient between predicted results and the test data

Angle of attack	Cavity water tunnel test data	Predicted results	Error/%
2°	0.115	0.112	2.8
4°	0.2589	0.246	4.9
8°	0.5141	0.473	7.9

Table.2 The compare of pressure center coefficient between predicted results and the test data

Angle of attack	Wind tunnel test data	Predicted results	Error/%
2°	0.57442	0.555	3.3
4°	0.52976	0.450	5.7
8°	0.45342	0.415	8.5

Table.1 and table.2 show that the predicted results agree closely near the cavity water tunnel test data, with the normal force coefficient error between predicted results and the cavity water tunnel test data 2%-8% and the pressure center coefficient error between predicted results and the wind tunnel test data 3%-9%. The error increases with the vehicle angle of attack increases. The validity of calculation model for no cavity flow is verified.

3.2 Reasonability for partial cavity flow model

To verify the validity of calculation model for with partial cavity flow, this paper compares the predicted results with the experiment data (from Ref.5). The comparison of cavity shape and pressure coefficients between predicted results and the test data at cavitation number of 0.3 and attack angle of 4 ° as follows:

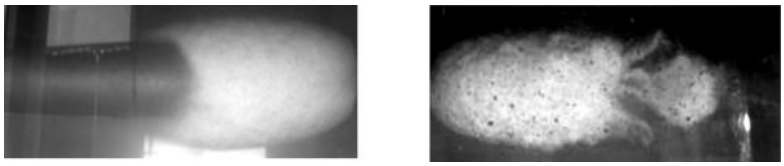

a) Cavitation in tunnel test (reference[5])

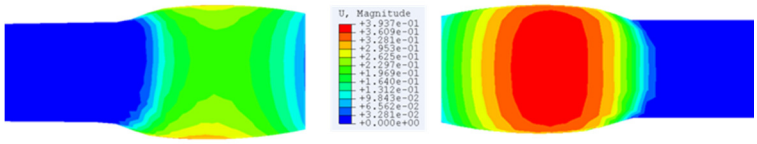

b) Cavitation of potential flow calculation

Figure 3: The contrast of cavitation between calculation and tunnel test (Left is front flow surface)

Once the cavity shape has been found, the pressure coefficient on the vehicle surface can be calculated according to:

$$C_p = \frac{p - p_\infty}{\frac{1}{2}\rho v^2} \tag{10}$$

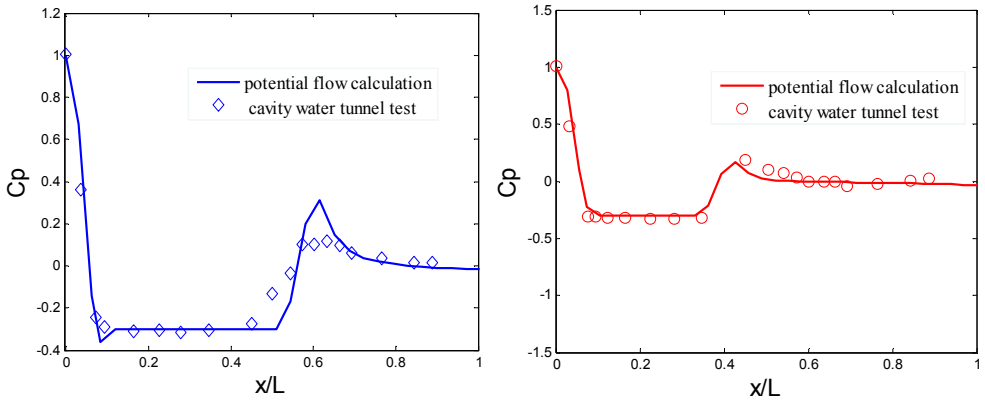

a) Back flow surface b) Front flow surface

Figure 4: The compare of Cp between Potential flow calculation and tunnel test

Fig.3 shows that the cavity shape is anisomerous at an attack angle, presenting phenomenon that the front flow surface of the partial cavity is short and thin and the other side is long and thick. The potential flow calculation result and the cavity water tunnel test result have a good agreement.

The pressure coefficient is plotted in Fig.4. Also shown in this figure is the cavity water tunnel test results. As we can see from Fig.4, the pressure coefficient given by the calculation agrees very well with the water tunnel test result both at the back flow surface and the front flow surface. The validity of calculation model to the hydrodynamic load of the vehicle at partial cavity flow is verified. We will do the following analysis based on the calculation method.

4 NUMERICAL RESULTS

4.1 Results of no cavity flow

In this section we will present some results of the surface pressure of the vehicles with different head shapes based on the effective calculation model for no cavity flow. All the vehicles' length is 10m, and the radius is 1m. All heads are semi-ellipsoids distinguished by the parameter shaft-section ratio a / b . As Fig.5 shows that b is the vehicle radius, which is a parameter. a is vehicle head length.

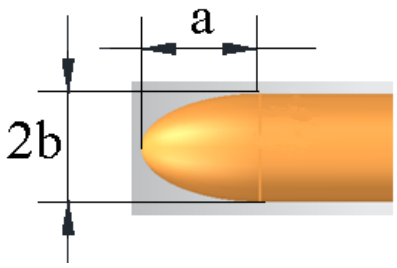

Figure 5: The Sketch of different head shapes' parameters

The normal force coefficients and pressure center coefficient results at attack angle of 2°of different type heads are presented in Tab.3.

Table.3 The result of normal force and pressure center coefficient for different type head

head shape parameters a/b	0.4	0.6	0.8	1.0	1.2
normal force coefficient	0.112	0.110	0.111	0.112	0.113
pressure center coefficient	0.472	0.468	0.465	0.463	0.463
head shape parameters a/b	1.4	1.6	1.8	2.0	
normal force coefficient	0.113	0.114	0.115	0.116	
pressure center coefficient	0.463	0.463	0.463	0.462	

Fig.3 shows that the normal force coefficient has a non-linear relationship with the head type parameter, and the coefficient increases very slowly in the a/b range of 1.0-1.8. When a/b=0.6, the coefficient has a minimum value 0.110. The pressure center coefficient is gradually reduced with a/b increases, and the pressure center move to the head position of the vehicle gradually.

4.2 Results with partial cavity flow at different cavitation number

In this section we will present the influence of different cavitation number to the vehicle's partial cavity hydrodynamic characteristic. The characteristic of the cavity flow around a vehicle with a cone head at various cavitation number at attack angle of 4 °.

The circumferential cavitation lengths and thickness under different cavitation number are plotted in Fig.6 and Fig.7.

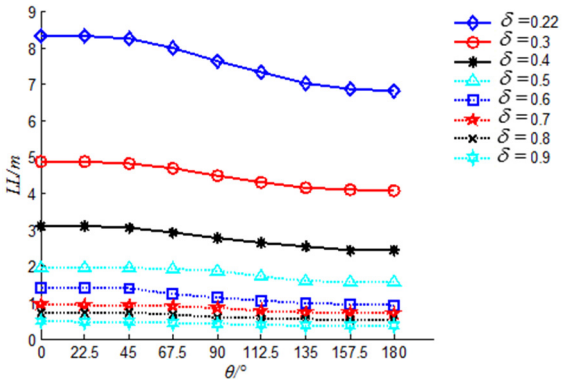

Figure 6: The circumferential curve of cavitation length under different cavitation number

Hence, we can draw the following conclusion based on Fig.6: the less the cavitation number is, the longer the length of the cavity is, and the cavity length is rising substantially at an exponential rate. When the cavitation number is 0.22, the cavity length at 0° position is almost close to the length of the entire vehicle. It is foreseeable that if cavitation number continues to decrease, the supercavitation will appear around the vehicle. When the cavitation number is 0.9, the cavity length is very small. It is also foreseeable that if cavitation number continues to increase, there will not be cavity around the vehicle. Meanwhile, the asymmetry of the cavity is more serious with the cavitation number reducing.

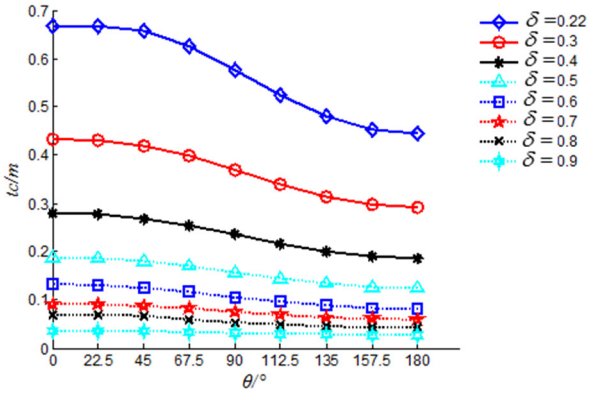

Figure 7:The circumferential curve of cavititation maximum thickness under different cavitation number

Fig.7 shows that the less the cavitation number is, the thicker the maximum thickness of the cavity is, and the cavity thickness is rising substantially at an exponential rate. Moreover, the smaller the cavitation number, circumferential cavity thickness difference is becoming greater. When the cavitation number is 0.22, the difference can reach to 0.22m. This shows that for the vehicle with a 45° cone head, the cavitation number is smaller, the difference between the cavity length and the thickness of the cavity are increased, which the asymmetry of the cavity becomes more serious.

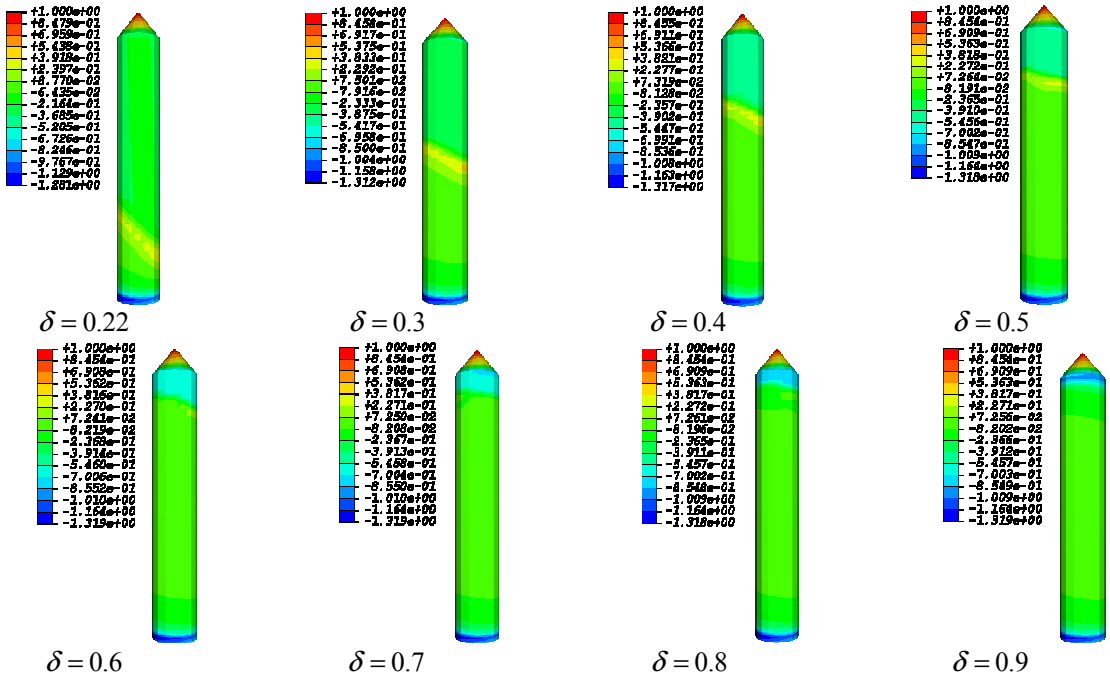

Figure 8: The nephogram of Cp under different cavitation number

Fig.8 shows that the cavity becomes thin and short with the increase of the cavitation number. The asymmetry of the cavity becomes more serious with the decrease of the cavitation number.

The pressure coefficient at front flow surface and back flow surface are plotted in Fig.9 and Fig.10.

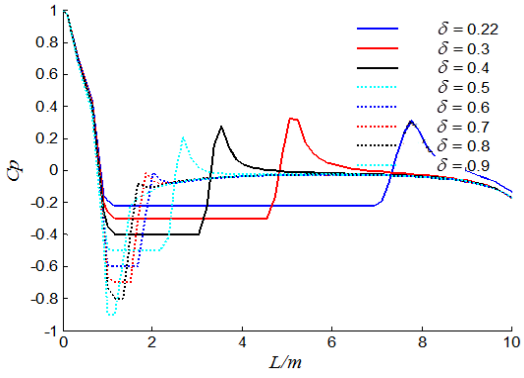

Figure 9: The curve of *Cp* at front flow surface under different cavitation number

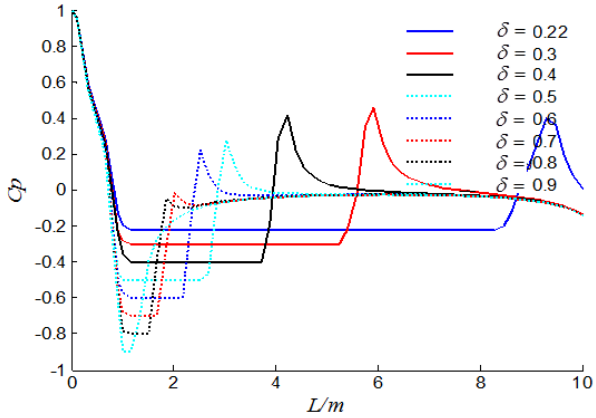

Figure 10: The curve of *Cp* at back flow surface under different cavitation number

Fig.9 and Fig.10 show that the cavity pressure has a rapid decline at the head of vehicle, and there will be cavity at the shoulder of vehicle. The length of the cavity termination zone becomes longer, and the pressure peak in it becomes higher with the decrease of the cavitation number.

5 CONCLUSION

On the basis of the Potential Flow Theory, the paper deduces and establishes mathematical calculations of the characteristic of cavity flow around underwater 3D vehicle. By comparing the results of numerical calculation with the experiment, the reasonability of the procedure was validated. On the basis of it, the paper analyzed the effects of different head shape and different cavitation number to the characteristics of flow around underwater vehicle, some conclusions are obtained:

1) As for no cavity flow, the predicted results agree closely near the cavity water tunnel test data, with the normal force coefficient error between predicted results and the cavity water tunnel test below 8% and the pressure center coefficient error between predicted results and the wind tunnel test data blow 9%.

2) As for partial cavity flow, the cavity shape and pressure coefficient given by the calculation agree very well with the water tunnel test result. The reasonability of the model is validated.

3) As for no cavity flow, the normal force coefficient has a non-linear relationship with the head type parameter, and the coefficient decreases then increases very slowly in the a/b range of 1.0-1.8. When a/b=0.6, the coefficient has a minimum value 0.110. The pressure center coefficient is gradually reduced with a/b increases, and the pressure center move to the head position of the vehicle gradually.

4) As for partial cavity flow, the cavity becomes long and thick, and the asymmetry of the cavity becomes more serious with the decrease of the cavitation number.

ACKNOWLEDGMENTS

This paper is funded by the International Exchange Program of Harbin Engineering University for Innovation-oriented Talents Cultivation.

REFERENCES

[1] MAYA. Water entry and cavity-running behaviour of missiles [R].AD-A020259, (1975).
[2] HU X. and GAO Y. Numerical investigation on supercavity shape control for underwater vehicles. *Journal of Harbin Engineering University* (2011) **32**(12):1556-1562.
[3] SINGHAL A. K. and ATHAVALE M. M. Mathematical basis and validation of the full cavitation model. *Journal of Fluids Engineering* (2002) **12**: 617-624.
[4] Quan X. B. and Zhao C. J. Numerical simulation of flow around underwater vehicle. *Journal of Ship Mechanics* (2006) **10**: 44-48.
[5] Quan X. B. and Li Y. An experiment study on cavitation of underwater vehicle's surface at large angles of attack. *Chinese Journal of Hydrodynamics* (2008) **23**: 662-667.
[6] Leng H.J. and Lu C.J. Study on Partially Cavitating Flow of an Axisymmetric Body. *Journal of Shanghai Jiaotong University* (2002) **36**(3):395-398.
[7] Hanaoka Tatsuro. Linear Theory of Cavitation Flow Field of Any Airfoil Ⅲ: Solution to Partial Cavity. *Proceedings of Society of Japanese Naval Architects* (1966) **119**:18-27.
[8] Liu J.B. and Xiao C.R. Numerical computation of cavitating flow around axisymmetric bodies. *Journal of Naval University of Engineering* (2004) **16**(4):4-7.
[9] Dai Y. S. and Duan W. Y. Potential Flow Theory of Ship Motions in Waves [M]. *National Defense Industry Press* (2006) **2**nd. 56-80.
[10] Zhang A. M. and Yao X. L. The interaction between multiple bubbles and the free surface. *Chinese Physics B* (2008) **17**(03):927-938.
[11] Zhang Z. Y. and Yao X. L. Cavitation shape of the three-dimensional slender at a small attack angle in a steady flow. *Acta Phys. Sin.* (2013) **62**(20): 20770101-09.